# On the origin of grain size effects in Ba(Ti$_{0.96}$Sn$_{0.04}$)O$_3$ perovskite ceramics

Yongqiang Tan, [1,2] Giuseppe Viola, [3,4] Vladimir Koval,[5] Chuying Yu,[3] Amit Mahajan,[3] Jialiang Zhang,[2] Haibin Zhang,[1, *] Xiaosong Zhou,[1] Nadezda V. Tarakina,[3] and Haixue Yan[3,*]

[1]*Innovation Research Team for Advanced Ceramics, Institute of Nuclear Physics and Chemistry, China Academy of Engineering Physics, Mianyang, 621900, China*
[2]*School of Physics, State Key Laboratory of Crystal Materials, Shandong University, Jinan, 250100, China*
[3]*School of Engineering and Materials Science, Queen Mary University of London, Mile End Road, London, E1 4NS, United Kingdom*
[4]*Department of Applied Science and Technology, Institute of Materials Physics and Engineering, Corso Duca Degli Abruzzi 24, 10129 Torino, Italy*
[5]*Institute of Materials Research, Slovak Academy of Sciences, Watsonova, 47, 040 01 Kosice, Slovakia*

## Abstract

Over the last 50 years, the study of grain size effects in ferroelectric ceramics has attracted great research interest. Although different theoretical models have been proposed to account for the variation in structure and properties of ferroelectrics with respect to the size of structural grains, the underlying mechanisms are still under debate. Here, we report the results of a study on the influence of grain size on the structural and physical properties of Ba(Ti$_{0.96}$Sn$_{0.04}$)O$_3$ (BTS), a ferroelectric compound that represents a model perovskite system, where the effects of point defects, stoichiometry imbalance and phase transitions are minimized by chemical substitution. It was found that different microscopic mechanisms are responsible for the different grain size dependences observed in BTS. High permittivity is achieved in fine-grained BTS ceramics due to high domain wall density and polar nanoregions; high d$_{33}$ is obtained in coarse-grained ceramics due to a high degree of domain alignment during poling; large electric field-induced strain in intermediate-grained ceramics is an outcome of a favorable interplay between constraints from grain boundaries and reversible reorientation of non-180º domains and polar nanoregions. These paradigms can be regarded as general guidelines for the optimization of specific properties of ferroelectric ceramics through grain size control.

**Corresponding Authors**:

*Haibin Zhang. Email: hbzhang@caep.cn  *Haixue Yan. Email: h.x.yan@qmul.ac.uk

# 1. Introduction

The study of grain size effects in polycrystalline ferroelectrics has drawn great interest in the past decades and it still represents a hot topic in the area of ferroelectrics [1-11]. The majority of studies on grain size effects currently available in the literature are mainly focused on two aspects. One concerns the investigation of ferroelectric properties in nanometer-scale structures and it is devoted to clarifying the size limits of ferroelectricity [12-16]. The other aspect is mainly related to the understanding of the grain size dependence of dielectric, piezoelectric and ferroelectric/ferroelastic behavior in bulk systems, aimed at obtaining desired properties by an appropriate tailoring of the grain size [4,6,9,10,17-25].

Regarding the grain size effects on dielectric properties, barium titanate ($BaTiO_3$) is probably the most widely studied material among ferroelectric ceramics [2, 4-6, 8, 17, 18, 23, 24, 26, 27]. The permittivity of $BaTiO_3$ ceramics generally shows a peak value around the grain size of 1 μm, regardless of the raw materials and sintering methods used [8,17-18]. The origin of the permittivity peak has been commonly attributed to the maximum density and mobility of 90º domain walls [6, 8,17,18, 24, 27].

Although grain size effects in ferroelectrics have been extensively studied, a satisfactory understanding of all the trends observed has not been achieved yet. In fact, large discrepancies in the grain size dependences of piezoelectric properties have been reported for different ferroelectric systems [6, 8-10, 19, 21-25, 27]. Even for pure $BaTiO_3$ ceramics, just the use of different raw materials and different sintering methods may lead to completely different grain size dependencies of the piezoelectric coefficients [6, 8, 23, 24, 26, 27]. The origin of the diverse grain size dependencies can be ascribed to intrinsic factors, such as crystal structure and phase coexistence, as well as extrinsic factors, including the degree of domains' alignment and the presence of charged point defects [8, 21, 28, 29]. In particular, a significant influence of point defects on grain size effects has been recently demonstrated by comparing the electrical properties of $BaTiO_3$ ceramics prepared by pressure-less sintering and spark plasma sintering (SPS) [8].

In order to fully understand the effects of grain size on macroscopic properties of ferroelectrics, high purity systems, with a high degree of stoichiometric balance and with the minimal presence of defects, are needed. During our compositional screening, it was noticed that the formation of point defects in $BaTiO_3$ ceramics during sintering at high temperatures can be suppressed by the substitution of $Ti^{4+}$ with the isovalent $Sn^{4+}$ or $Zr^{4+}$ ions [30,31]. Besides that, the addition of $Sn^{4+}$ or $Zr^{4+}$ions allows for shifting the temperatures of the phase transitions from the rhombohedral *R3m* to the orthorhombic *Amm2* phase and from the orthorhombic *Amm2* to the tetragonal *P4mm* structure [32-37]. This enables studying grain size effects in stable phases, sufficiently far from phase transition temperatures.

In this paper, $Ba(Ti_{0.96}Sn_{0.04})O_3$ (abbreviated as BTS hereafter) ceramics were prepared to study the effect of grain size on the phase composition, crystal symmetry, domain structure, dielectric permittivity, piezoelectric $d_{33}$ coefficient and ferroelectric/ferroelastic properties with minimal influence of the point defects, stoichiometry imbalance and phase transition critical behavior. The results obtained contribute to a more comprehensive understanding of the grain size effects in ferroelectric ceramics; knowledge that could enable preparing functional electronic materials with improved dielectric, piezoelectric and ferroelectric/ferroelastic properties.

## 2. Experimental

## 2.1 Sample preparation

$Ba(Ti_{0.96}Sn_{0.04})O_3$ ceramics were prepared using $BaCO_3$ (SINOPHARM, China, purity $\geq$ 99.0%), $TiO_2$ (SINOPHARM, China, purity $\geq$ 99.8%) and $SnO_2$ (SINOPHARM, China, purity$\geq$99.8%) powders, which were weighed according to the stoichiometric formula and thoroughly mixed. The homogenized mixture was then ball-milled for 12 hrs in alcohol and calcined at 1050°C for 4 hrs. After calcination, the BTS powder was ball-milled again for 12 hrs. Dense BTS ceramics with different grain sizes were obtained by sintering at different temperatures in the range of 1160 - 1320°C under a uniaxial pressure of 85 MPa for 5 minutes using a commercial SPS furnace (HPD-25/1 FCT Systeme GmbH). The ceramic samples sintered at 1160°C, 1200°C, 1240°C, 1280°C and 1320°C are labeled as BTS1160,

BTS1200, BTS1240, BTS1280, and BTS1320, respectively, throughout the manuscript. The SPS-processed samples (denoted as SPSed hereafter) were further annealed in air at 1000°C for 2 hrs in order to remove the carbon diffused in the samples during SPS sintering.

## 2.2 Microstructural characterizations

The microstructure of the ceramics was studied using scanning and transmission electron microscopy. Scanning electron microscopy (SEM) was performed on polished and chemically etched samples using a scanning electron microscope (JEOL, model JSM 6300). The etching was performed in an aqueous solution of 5% HCl with a small amount of HF (3 drops of HF: 20 ml HCl solution) for 10 seconds. Transmission electron microscopy (TEM) was performed using a JEOL JEM 2010 microscope operated at 200 kV. Thin lamellas for TEM observations were prepared by focused ion beam milling using an FEI Quanta 3D Dual Beam system (operational conditions: 30 kV Ga+ ion beam and currents down to 28 pA). When the thickness of the lamellas was about 100 nm, a final cleaning of the specimens was performed at 5 kV and 16 pA.

The local out-of-plane piezoresponse was measured using a scanning probe microscope (Ntegra Prima, NT-MDT) equipped with an external lock-in amplifier (SR 830, Stanford Research). A conductive probe (MikroMasch HQ: NSC15/Pt) working at the resonance frequency of 325 kHz and a force constant of 40 N/m was used for the acquisition of the piezoresponse data. The signals were recorded at 10 V and 50 kHz.

## 2.3 XRD tests and refinements

The crystal structure of the samples was studied by X-ray diffraction (XRD). XRD data were collected on an automated Rigaku X-ray diffractometer (model Ultima IV) with Cu $K_\alpha$-radiation in the $2\theta$ range $20° \leq 2\theta \leq 60°$ and at temperatures -100°C, 25°C, 75°C and 147°C. The Rietveld refinement of the crystal structure was performed with the FullProf software package [38,39]. The experimental profiles acquired at $2\theta$-diffraction angles from $10°$ up to $120°$ were fitted with the Thompson-Cox-Hastings pseudo-Voigt analytical function. The goodness of fit was used as a numerical criterion to assess the

quality of the diffraction data fitting.

## 2.4 Electrical characterizations

For the electrical characterization, ceramic specimens were coated on the top and bottom surfaces with silver paste, which was fired at 600°C for 20 minutes. The relative dielectric permittivity was measured using a precision impedance analyser (Agilent, a model 4294A) connected to a chamber with controlled temperature. The room-temperature polarization-electric field (P-E) hysteresis loops and strain-electric field (S-E) loops were measured with triangular electric-field waveforms of 3 kV/mm amplitude and a frequency of 1 Hz using a ferroelectric tester (NPL, Teddington, UK) [40]. The poling was carried at 95°C in silicon oil under a dc field of 3 kV/mm for 30 min. The piezoelectric $d_{33}$ coefficient was measured using a Berlincourt-type $d_{33}$ meter (YE 2730A, China).

## 3. Results and discussions

Figs. 1a - e show the micrographs of the polished and chemically etched surfaces of the BTS ceramics sintered at five different temperatures. All the samples investigated have low porosity and consistently high relative densities (> 98%), as measured by the Archimedes method. The average grain size increases from 0.8 μm to 12.5 μm as the sintering temperature increases from 1160°C to 1320°C (Fig. 1f). In fine-grained BTS ceramics, the typical stripe-like domain structure, commonly observed in fine-grained $BaTiO_3$ ceramics [8], is not clearly distinguished (Fig. 1a and 1b). It appears that the grains contain separated domain islands instead of stripe domains. The peculiar domain morphology may result from a disruption of stripe-type domains by the reducing grain size. As the grain size increases, the presence of domains becomes increasingly neater (Fig. 1c - 1e). In coarse-grained BTS ceramics, the domain patterns are clearly visible (Fig. 1d and 1e). The watermark-type regions correspond to the 180° domains, while the stripe-type areas represent non-180° domains [41,42].

The presence of domains in micrometer-sized grains of the BTS1160 sample is evidenced by TEM (Fig. 2 and S1). Fig. 2a shows the dark-field TEM image of an area of several grains. From the image contrast, one can see that the central grain consists of three domains: two twin domains (areas

5

marked by "A" and "D") and a domain between them (corresponding to the bright area between "B" and "C"). The latter domain shows superstructure reflections in the selected-area diffraction (SAED) pattern. The superstructure can be described in a rhombohedral lattice with the unit cell parameters (in hexagonal settings) $a$ = 6.5 Å and $c$ =12.7 Å (Fig. 2B and 2C). The two twin domains are rotated by 30° with respect to each other, as evidenced in the corresponding SAED patterns (Fig. 2A - D). A similar domain structure is observable also on the right side of the grain located in the bottom left corner of Fig. 2a and 2b (the area marked by "F" in Fig. 2b and 2F). However, the SAED pattern from the left side of the same grain (marked by "E" in Fig. 2b and 2E) presents extra spots along the [1-10] direction of the crystal. In both cases, the formation of different superstructures is most probably related to local cation ordering controlled by an inhomogeneous distribution of Sn [32]. Since the difference in the unit cell parameters of the orthorhombic BTS (space group *Amm*2) and the tetragonal BTS (space group *P4mm*) unit cells is less than 0.01 Å, the structure cannot be unambiguously distinguished from the SAED patterns (the indexing of the SAED patterns has been performed based on the tetragonal unit cell).

Piezoresponse force microscopy (PFM) was used to investigate the domain structure in BTS1160 and BTS1280. The dark and bright areas in the phase images (Fig. 3) correspond to domains with polarization oriented parallel (marked by green circles in Fig. 3b) and antiparallel (marked by blue circles in Fig. 3b) to the applied field, respectively. BTS1160 shows a mosaic-like pattern with sub-micrometer sized domains, along with the possible presence of polar nanoregions (PNRs), as illustrated by the phase image in Fig. 3c and the corresponding line profile in Fig. 3d. These images provide further details of the domain patterns observed in the micrographs (Fig.1a and 1b). The mosaic-like domain configuration and PNRs resembles the patterns characteristic of relaxor ferroelectrics [43]. The observation of a mosaic-like pattern clearly proves that even the BTS ceramic with the smallest grains here studied presents a multi-domain configuration within a single grain. The phase images of BTS1280 (Fig. 3f and 3g) demonstrate the presence of stripe-like domains, which is in accordance

with the SEM observations (Fig. 1d). The average domain size, as determined from the line profile in Fig. 3h (corresponding topography is presented in Fig. 3e), is ~ 1.4µm.

Figure 4 presents the phase compositions of the BTS ceramics with small (BTS1160), intermediate (BTS1240) and large (BTS1320) grains. The refined lattice parameters and *R*-factors, as obtained from the Rietveld analysis of the XRD data measured at four different temperatures (Fig. S2), are summarized in Table S1 (in Supplementary material). At -100°C, all the samples (BTS1160, BTS1240 and BTS1320) present the coexistence of rhombohedral (*R3m*) and orthorhombic (*Amm2*) phases (Fig. 4a), with the latter being dominant in the fine-grained ceramic BTS1160. At 25°C, the latter shows a pure orthorhombic structure (Fig. 4b). As the grain size increases the amount of tetragonal phase increases, so that the coarse-grained BTS1320 ceramic appears as a mixture of the orthorhombic structure (*Amm2*) and the tetragonal phase (*P4mm*) (Fig. 4b). The occurrence of the bi-phasic structure is in agreement with previous studies on pure $BaTiO_3$ [2, 35] and Sn-modified $BaTiO_3$ ceramics [34]. It can be inferred that the orthorhombic structure is favoured over the tetragonal phase in fine-grained BTS ceramics probably because it offers a higher number of directions for the spontaneous polarization, which helps to minimize the energy of the system [2]. This is also consistent with the shift of $T_{O-T}$ towards higher temperatures with decreasing grain size in $BaTiO_3$ ceramics, when the grain size is below 500 nm, based on a theoretical model [44]. At 75°C, BTS1160 exhibits the coexistence of orthorhombic and tetragonal phases; however, with increasing grain size, the orthorhombic phase disappears in favour of the tetragonal symmetry (Fig. 4c). The tetragonality (*c/a*) increases along the grain size, as can be seen in Table S1. The Rietveld analysis of the XRD data collected at 147°C (see Fig. S3) suggests the presence of a tetragonal/pseudocubic phase alongside the main cubic structure (*Pm-3m* space group symmetry) in all samples investigated. From Table S2 and Table S3, one can see that the refinements with a mixed *Pm*-3*m*+*P4mm*+*Fm*-3*m* model gave better values of the *R*-factors than those with the *Pm*-3*m*+*Fm*-3*m* model (e.g., $R_w/R_{wp}$ is 7.4/10.4 and 8.14/11.1 for the mixed structural model and the *Pm*-3*m*+*Fm*-3*m* model, respectively, for the BTS1160

sample). It should be noted that the *Fm-3m* phase contribution is from a platinum holder, which was used in X-ray diffraction measurements at elevated temperatures. In addition, the goodness of fit (GOF) factor was substantially improved when the mixed structural model was employed (in Tables S1 and S2 for BTS1160; GOF (*Pm-3m+P4mm+Fm-3m*) ~ 1.5 *vs*. GOF (*Pm-3m+Fm-3m*) ~ 2.1). Regarding the phase coexistence (*Pm-3m+P4mm*) at temperatures above the Curie point, the XRD results are in accordance with earlier structural studies which have demonstrated the coexistence of a displacive and order-disorder component in the phase transition mechanism of $BaTiO_3$ around the Curie point by means of nuclear magnetic resonance (NMR) spectroscopy [45], in-situ Raman spectroscopy [46], inelastic light scattering [47] and high-pressure Raman scattering [48]. It is generally accepted that a tetragonal-type breaking of the cubic symmetry is due to the biased Ti motion between the off-center sites in the paraelectric phase above $T_c$. In addition, local polar nanoregions were also observed in the ferroelectric and paraelectric phases of $BaTiO_3$ using a picosecond soft x-ray laser speckle technique [49].

Fig. 5a - f show the temperature dependences of the relative dielectric permittivity and loss of unpoled BTS ceramics with different grain size. Similarly to pure $BaTiO_3$ ceramics, three dielectric anomalies can be identified in the temperature range investigated (-50°C-150°C), which correspond to the rhombohedral-to-orthorhombic ($T_{R-O}$), orthorhombic-to-tetragonal ($T_{O-T}$) and tetragonal-to-cubic ($T_C$) phase transitions. The dielectric anomalies associated with the phase transitions are much more pronounced in coarse-grained samples (Fig. 5e and 5f), while for fine-grained ceramics (Fig. 5a and 5b) only the Curie point $T_C$ can be clearly identified. From the temperature dependence of the relative dielectric permittivity, it was difficult to determine the grain size dependence of $T_{R-O}$. More obvious sensitivity to a variation in grain size can be observed in the structural transformation temperature from the orthorhombic to the tetragonal phase. $T_{O-T}$ gradually shifts to a higher temperature by decreasing the average grain size. The Curie point $T_C$ does not show a significant grain size dependence when the

grains are larger than 2.2μm. In comparison with pure $BaTiO_3$ [8], all the BTS samples show higher $T_{R-O}$ and $T_{O-T}$ temperatures, while lower $T_C$.

In BTS1160, the permittivity peak around $T_C$ slightly broadens and it displays tiny shifts towards higher temperatures with increasing frequency (see inset of Fig. 5a). These observations are in agreement with previous data on $Ba(Ti_{1-x}Sn_x)O_3$ ceramics with x > 0.19 [50-53]. In BTS1320, the permittivity peak at $T_C$ shows a negligible dependence on the frequency (inset of Fig. 5e). From Fig.4c and Table S2 and S3, one can notice that BTS1160 experiences a transition from (*Amm2+P4mm*) to (*P4mm+Pm-3m*) across $T_C$, while the intermediate and large grain ceramics undergo a transition from *P4mm* to (*P4mm+Pm-3m*).This is probably the reason why the ferroelectric–paraelectric transition is more diffuse in the fine grain ceramic.

When the temperature is above $T_C$, the permittivity of BTS ceramics shows no grain size dependence (Fig. 5g). At $T_C$, where the contribution of domain walls density to the net polarization usually vanishes, the dielectric permittivity decreases with decreasing grain size (Fig. 5g), as a result of the increased number of grain boundaries with low permittivity. Upon cooling through the paraelectric-ferroelectric phase transition, the dielectric permittivity shows clear grain size dependence. In all ferroelectric phases, the permittivity increases with decreasing the average grain size down to 0.8μm (Fig. 5g). This can be attributed to the increased presence of domain walls and PNRs in the ceramics with small grain size.

The dielectric loss above $T_C$ of all BTS ceramics are less than 0.01, suggesting that the formation of point defects during sintering at high temperatures was hindered by $Sn^{4+}$ doping. Therefore, the influence of point defects on the grain size dependences observed in this study can be neglected. The reduced concentration of point defects in BTS ceramics is also demonstrated by the temperature dependence of the permittivity measured up to 800°C (Fig. S4). The permittivity peak around 600°C, related to the presence of oxygen vacancies in perovskites [54], was significantly suppressed even in the BTS ceramic sintered at 1320°C, if compared to the dielectric behaviour of pure $BaTiO_3$ ceramics

[8]. It has been previously reported that the presence of oxygen vacancies in $BaTiO_3$ is strongly related to the unstable valence state of $Ti^{4+}$ [55]. A partial substitution of $Ti^{4+}$ with more chemically-stable $Zr^{4+}$ was theoretically and experimentally proved to decrease the amount of oxygen vacancies in $BaTiO_3$ [30,31]. Taking in account the similarities between the chemical stability of $Zr^{4+}$ and $Sn^{4+}$ cations [34], the inhibiting effect of $Sn^{4+}$ addition on the formation of oxygen vacancies in BTS can be explained.

The polarization-electric field (P-E) loops and the current-electric field (I-E) curves of BTS ceramics sintered at three different temperatures (1160°C, 1240°C and 1320°C) are shown in Fig. 6. Figs. 6a - c show the P-E and I-E loops traced at room temperature, while those recorded at 125°C are presented in Fig. 6d, 6e and 6f. It can be seen that at room temperature, all the BTS samples show typical ferroelectric P-E loops. With increasing grain size, the loops become increasingly more saturated. The values of $P_{max}$ and $P_r$ of BTS1160 (average grain size 0.8 µm) are 20.4 µC/cm$^2$ and 7.9 µC/cm$^2$, respectively. As the grain size increases from 0.8 µm to 12.5 µm, $P_{max}$ slightly increases from 20.4 µC/cm$^2$ to 21.3 µC/cm$^2$, and $P_r$ sharply increases to 14.5 µC/cm$^2$, which is almost twice the value found in BTS1160 ceramics (7.9 µC/cm$^2$). The observed dependences of $P_{max}$ and $P_r$ on the grain size are in good agreement with those earlier reported for the $BaTiO_3$ ceramics prepared by SPS from nano-sized powders [8,56]. The coercive field continuously decreases with increasing grain size from 0.314 kV/mm in BTS1160 to 0.138 kV/mm in BTS1320.

It is worth mentioning that all ceramics show signs of domain switching even at 125°C (> $T_C$ ~ 105°C), as evidenced by the tiny current peaks in the I-E curve (Figs. 6d - f), which can be attributed to the reorientation of polar regions which might be still present above $T_C$ in $BaTiO_3$-based materials [53, 57, 58]. In the coarse-grained BTS1320 ceramic, the domain switching current peak above $T_C$ becomes clearly suppressed (Fig. 6f). The temperature dependences of the maximum and remanent polarization of BTS1160, BTS1240 and BTS1320 are shown in Fig. 6g. With increasing temperature,

$P_{max}$ and $P_r$ slightly decrease until 50°C; at higher temperature, a significant decrease of both quantities is observed in all the three ceramics investigated.

Fig. 7a presents the room-temperature strain-electric field (S-E) loops (without including the first poling cycle) of BTS ceramics with different grain size. It can be seen that all the S-E curves exhibit a typical butterfly-like shape with symmetrical wings, even for the samples sintered at high temperature. This is quite different from the bipolar S-E curves shown by pure $BaTiO_3$ ceramics, which evidenced a remarkable tendency to become asymmetrical when the sintering temperature is higher than 1200°C [8, 59]. The asymmetry is commonly attributed to the development of an internal bias due to hindering of the domain wall movement by point defects [8, 59-61]. The symmetrical S-E loops in BTS ceramics may further validate the hypothesis that a small amount of $Sn^{4+}$ addition might suppress the formation of point defects, such as oxygen vacancies, during sintering at high temperatures. From Fig. 7a it can be seen that with increasing grain size the strain amplitude in the bipolar test gradually increases until a maximum value of about 0.2%, observed at 2.2 µm average grain size, beyond which the strain amplitude drastically decreases. Fig. 7b shows the unipolar S-E curves of dc-poled BTS ceramics with different grain size. The measurements were carried out by setting at zero the remanent strain after the poling process. All dc-poled BTS ceramics show slim unipolar S-E loops with a nearly zero remanent strain. Similarly to the bipolar strain curves, the maximum strain achieved in the unipolar test first increases and then decreases with increasing grain size, showing a peak value of 0.23% at 2.2 µm grain size. The strain-polarization (S-P) loops of BTS ceramics with three different grain size (0.8 µm, 2.2 µm and 12.5 µm) are shown in Fig. 7c. BTS1160 (grain size: 0.8 µm) shows a slim S-P loop without hysteresis, indicating that in the fine-grained BTS ceramic the dominant contribution to both polarization and strain might be given by non-180° domains and PNRs [40,62]. The S-P loop of BTS1280 with 2.2 µm grains shows a small hysteresis, suggesting that non-180° domains or PNRs still play a dominant role in the ceramic sample, while the contribution of 180° domains is negligible [8, 40]. For the coarse-grained BTS1320 ceramic with 12.5 µm grain size, the hysteresis of the S-P loop

becomes prominent. Additionally, the polarization becomes larger and the strain significantly reduces, indicating that the extent of 180º domain switching is much larger than that occurring in fine-grained BTS ceramics. Fig. 8 summarizes the grain size dependencies of the dielectric and piezoelectric characteristics. The dependence of the relative dielectric permittivity on grain size at three specific temperatures (-50 °C, 25 °C and 50 °C) in Fig. 8a was extrapolated from Fig. 5. The permittivity exhibits similar grain size dependencies in the three different phases: it keeps increasing with decreasing grain size without showing any peak in the grain size range studied. This is different from BaTiO$_3$ ceramics, which show a permittivity peak around 1 µm grain size [6, 8, 17, 24, 63]. The room-temperature dielectric permittivity of BTS1320 with an average grain size of 12.5 µm is about 2400, while it increases to about 3900 when the average grain size is decreased to 0.8 µm. The permittivity of all BTS ceramics decreases after dc poling; the decrease is larger in the coarse-grained sample (see Fig. 8b). This can be explained by the lower domain wall density in coarse-grained ceramics after poling [8].

The grain size dependence of the piezoelectric coefficient d$_{33}$ is shown in Fig. 8c. One can see that it exhibits a totally opposite grain size dependence compared to that of the relative dielectric permittivity at all the three temperatures considered. In ceramics with an average grain size of 0.8 µm, the d$_{33}$ at room temperature is 100 pC/N, and it gradually increases with increasing the average grain size. When the average grain size is 12.5 µm, the room-temperature d$_{33}$ reaches 380 pC/N, which is almost four times larger than that of the fine-grained BTS ceramic. The grain size dependences of the d$_{33}$ at different temperatures show similar trends. It should be noted that the piezoelectric coefficient increases with increasing temperature, approaching the orthorhombic-tetragonal transition ($T_{O-T}$ ~ 40 °C). Thermal depoling effects become significant only above 75 °C.

The room-temperature piezoelectric coefficient d$_{33}$$^*$ of poled BTS ceramics was calculated as the ratio $S_{max}/E_{max}$ [64] using the data in Fig. 7b. The grain size dependence of d$_{33}$$^*$ is presented in Fig. 8d. One can see that the d$_{33}$$^*$ first increases with increasing the average grain size, then it reaches a

maximum ($\sim$ 390 pm/V) at 2.2 μm, and it finally decreases with a further increase of the grain size, until a value of about 200 pm/V in BTS ceramics with an average grain size of 12.5 μm. The grain size dependence of the electric field-induced strain of BTS ceramics is quite similar to that of pure $BaTiO_3$ ceramics prepared from 100 nm $BaTiO_3$ powders by SPS [65].

From the obtained experimental results, it can be summarised that in BTS ceramics, where point defects do not have a significant influence on the trends observed, the dielectric permittivity, the piezoelectric coefficient and the electric field-induced strain show different grain size dependences. Fine-grained samples exhibit high dielectric permittivity; coarse-grained samples show higher $d_{33}$; samples with intermediate grain size can experience larger electric field-induced strain. This evidences that high dielectric permittivity, high piezoelectric constant and large electric field-induced strain in $BaTiO_3$-based ceramics originate from different physical mechanisms.

The experimental and theoretical studies of the grain size effect on the dielectric permittivity of $BaTiO_3$ ceramics have demonstrated that high permittivity is closely related to the maximized domain wall density in fine grains [6, 8, 17, 24, 52]. The observed grain size dependence of the permittivity in BTS ceramics is similar to that found in pure $BaTiO_3$ [8, 17, 24, 27], implying that the high density of domain walls plays an important role also in BTS ceramics. The main difference is that BTS ceramics show no permittivity peak in the range of grain size studied, while $BaTiO_3$ ceramics exhibit a permittivity peak around 1 μm grain size [6, 8, 17, 18, 24, 52]. Besides, in this study, the higher permittivity in fine-grained BTS ceramics can be also due to the presence of PNRs, which provide the main contribution to the high permittivity in relaxors [66, 67]. The grain size dependence of piezoelectric properties is mainly influenced by the mechanisms of domain switching and domain alignment under high electric fields [8, 21, 35]. BTS ceramics exhibit the presence of both 180º and non-180º domains; the former are pure ferroelectric and mainly contribute to the electrical polarization, while the latter are both ferroelectric and ferroelastic, and thus they can simultaneously contribute to polarization and strain. Additionally, there might be also a non-negligible contribution of PNRs to

13

polarization and strain. From the S-P curves of BTS ceramics with different grain sizes (Fig. 7c), it can be inferred that the amount of 180º domains increases with increasing grain size within the range studied. In addition, the increased remanent polarization in coarse-grained ceramics suggests that the driving force of back switching decreases with increasing grain size. These grain size-controlled features are thought to be responsible for the increase of the $d_{33}$ coefficients in poled BTS ceramics with larger grains due to the enhanced domain alignment after the poling process.

The domain switching process under high electric field can be partly reversible and partly irreversible [68-70]. The main contribution to the electric field-induced strain in bipolar tests is given by the reversible switching of non-180º domains and possibly by PNRs, when present [62, 69, 71, 72]. In fact, in some ferroelectric/ferroelastic ceramics, only a limited part of the strain produced during the very first electric field cycle applied on virgin samples can be recovered during field unloading and reversal [65, 69]. In coarse-grained BTS ceramics, a larger portion of non-180º domain switching is irreversible. This is also evidenced in Fig. 8b, which shows that the difference of the permittivity before and after poling gradually increases with increasing grain size, indicating the increased proportion of irreversible domain switching during poling. The increase of both the portion of 180º domains and the irreversible switching of non-180° domains lead to the decreased strain amplitude in coarse-grained BTS ceramics as shown in Fig. 8. In fine-grained BTS ceramics, the constraint from grain boundaries hinders domain switching [73]. Therefore, the largest amount of reversible field-induced processes occurs in ceramics with intermediate grain size, resulting from the convoluted contributions of the applied field, grain boundaries and temperature, which affect domain forward/backward switching and the stability of domains and PNRs.

## 4. Conclusion

By studying grain size effects in Ba(Ti$_{0.96}$Sn$_{0.04}$)O$_3$ ceramics, the present paper identifies the grain size dependence of the dielectric, piezoelectric and ferroelectric/ferroelastic properties that would be generally observed in bulk ferroelectrics, when the influence of point defects, non-stoichiometry and

phase transitions is minimized. High permittivity in fine grains is achieved by maximized density of domain walls and polar nanoregions; high $d_{33}$ in coarse-grained ceramics is determined by high degree of domain alignment after poling; large electric field-induced strain in intermediate-grained ceramics is due to a favourable combination of constraints from grain boundaries and reversible reorientation of non-180º domains and eventually polar nanoregions.

**Acknowledgements**

**References**

[1]  H. M. Duiker, P. D. Beale, Grain-size effects in ferroelectric switching, Phys. Rev. B 41 (1990) 490-495.

[2]  M. H. Frey, D. A. Payne, Grain-size effect on structure and phase transformations for barium titanate, Phys. Review B 54 (1996) 3158-3168.

[3]  V. Hornebecq, C. Huber, M. Maglione, M. Antonietti, C. Elissalde, Dielectric properties of pure $(BaSr)TiO_3$ and composites with different grain sizes ranging from the nanometer to the micrometer, Adv. Funct. Mater. 14 (2004) 899-904.

[4]  Z. Zhao, V. Buscaglia, M. Viviani, M. T. Buscaglia, L. Mitoseriu, A. Testino, M. Nygren, M. Johnsson, P. Nanni, Grain-size effects on the ferroelectric behavior of dense nanocrystalline $BaTiO_3$ ceramics, Phys. Rev. B 70 (2004) 024107.

[5]  L. Curecheriu, S. B. Balmus, M. T. Buscaglia, V. Buscaglia, A. Ianculescu, L. Mitoseriu, Grain size-dependent properties of dense nanocrystalline barium titanate ceramics, J. Am. Ceram. Soc. 95 (2012) 3912-3921.

[6]  D. Ghosh, A. Sakata, J. Carter, P. A. Thomas, H. Han, J. C. Nino, J. L. Jones, Domain wall displacement is the origin of superior permittivity and piezoelectricity in $BaTiO_3$ at intermediate grain sizes, Adv. Func. Mater. 24 (2014) 885-896.

[7]  F. Benabdallah, C. Elissalde, U. C. C. Seu, D. Michau, A. Poulon-Quintin, M. Gayot, P. Garreta, H. Khemakhem, M. Maglione, Structure–microstructure–property relationships in lead-free BCTZ piezoceramics processed by conventional sintering and spark plasma sintering, J. Eur. Ceram. Soc. 35 (2015) 4153-4161.

[8]  Y. Tan, J. Zhang, Y. Wu, C. Wang, V. Koval, B. Shi, H. Ye, R. McKinnon, G. Viola, H. Yan, Unfolding grain size effects in barium titanate ferroelectric ceramics, Sci. Rep. 5 (2015) 9953.

[9]  M. Muthuramalingam, D. E. Jain Ruth, M. Veera Gajendra Babu, N. Ponpandian, D. Mangalaraj, B. Sundarakannan, Isothermal grain growth and effect of grain size on piezoelectric constant of

$Na_{0.5}Bi_{0.5}TiO_3$ ceramics, Scripta Mater. 112 (2016) 58-61.

[10] D. K. Khatua, T. Mehrotra, A. Mishra, B. Majumdar, A. Senyshyn, R. Ranjan, Anomalous influence of grain size on the global structure, ferroelectric and piezoelectric response of $Na_{0.5}Bi_{0.5}TiO_3$, Acta Mater. 134 (2017) 177-187.

[11] J. Koruza, P. Groszewicz, H. Breitzke, G. Buntkowsky, T. Rojac, B. Malič, Grain-size-induced ferroelectricity in $NaNbO_3$, Acta Mater. 126 (2017) 77-85.

[12] D. D. Fong, G. B. Stephenson, S. K. Streiffer, J. A. Eastman, O. Auciello, P. H. Fuoss, C. Thompson, Ferroelectricity in ultrathin perovskite films, Science 304 (2004) 1650-1653.

[13] N. A. Spaldin, Fundamental size limits in ferroelectricity, Science 304 (2004) 1606-1607.

[14] H. Han, Y. Kim, M. Alexe, D. Hesse, W. Lee, Nanostructured ferroelectrics: fabrication and structure–property relations, Adv. Mater. 23 (2011) 4599-4613.

[15] P. M. Rørvik, T. Grande, M. A. Einarsrud, One-dimensional nanostructures of ferroelectric perovskites, Adv. Mater. 23 (2011) 4007-4034.

[16] M. J. Polking, M. G. Han, A. Yourdkhani, V. Petkov, C. F. Kisielowski, V. V. Volkov, Y. Zhu, G. Caruntu, A. Paul Alivisatos, R. Ramesh, Ferroelectric order in individual nanometre-scale crystals, Nat. Mater. 11 (2012) 700-709.

[17] G. Arlt, Dielectric properties of fine-grained barium titanate ceramics, J. Appl. Phys. 58 (1985) 1619-1625.

[18] G. P. Khanal, S. Kim, M. Kim, I. Fujii, S. Ueno, S. Wada, Grain-size dependence of piezoelectric properties in thermally annealed $BaTiO_3$ ceramics, J. Ceram. Soc. Jpn. 126 (2018) 536-541.

[19] T. M. Kamel, G. de With, Grain size effect on the poling of soft $Pb(Zr,Ti)O_3$ ferroelectric ceramics, J. Eur. Ceram. Soc. 28 (2008) 851-861.

[20] G. Viola, K. B. Chong, M. Eriksson, Z. Shen, J. Zeng, Q. Yin, Y. Kan, P. Wang, H. Ning, H. Zhang, M. E. Fitzpatrick, M. J. Reece, H. Yan, Effect of grain size on domain structures, dielectric and thermal depoling of Nd-substituted bismuth titanate ceramics, Appl. Phys. Lett. 103 (2013)

182903.

[21] C. A. Randall, N. Kim, J.-P. Kucera, W. Cao, T. R. Shrout, Intrinsic and extrinsic size effects in fine-grained morphotropic-phase-boundary lead zirconate titanate ceramics, J. Am. Ceram. Soc. 81 (1998) 677.

[22] H. Zhang, H. Yan, H. Ning, M. J. Reece, M. Eriksson, Z. Shen, Y. Kan, P. Wang, The grain size effect on the properties of Aurivillius phase $Bi_{3.15}Nd_{0.85}Ti_3O_{12}$ ferroelectric ceramics, Nanotechnology 20 (2009) 385708.

[23] S. Ding, T. Song, X. Yang, G. Luo, Effect of grain size of $BaTiO_3$ ceramics on dielectric properties, Ferroelectrics 402 (2010) 55.

[24] P. Zheng, J. L. Zhang, Y. Q. Tan and C. L. Wang, Grain-size effects on dielectric and piezoelectric properties of poled $BaTiO_3$ ceramics, Acta Mater. 60 (2012) 5022.

[25] J. Hao, W. Bai, W. Li, J. Zhai, Correlation between the microstructure and electrical properties in high-performance $(Ba_{0.85}Ca_{0.15})(Zr_{0.1}Ti_{0.9})O_3$ lead-free piezoelectric ceramics, J. Am. Ceram. Soc. 95 (2012) 1998.

[26] Y. Huan, X. Wang, J. Fang, L. Li, Grain size effects on piezoelectric properties and domain structure of $BaTiO_3$ ceramics prepared by two-step sintering, J. Am. Ceram. Soc. 96 (2013) 3369.

[27] Y. Huan, X. Wang, J. Fang, L. Li, Grain size effect on piezoelectric and ferroelectric properties of $BaTiO_3$ ceramics, J. Eur. Ceram. Soc. 34 (2014) 1445.

[28] M. Legallais, S. Fourcade, U. C. Chung, D. Michau, M. Maglione, F. Mauvy, C. Elissalde, C. Fast re-oxidation kinetics and conduction pathway in Spark Plasma Sintered ferroelectric ceramics, J. Eur. Ceram. Soc. 38 (2017) 543.

[29] F. Rubio-Marcos, J. F. Fernandez, D. A. Ochoa, J. E. García, R. E. Rojas-Hernandez, M. Castro, L. Ramajo, Understanding the piezoelectric properties in potassium-sodium niobate-based lead-free piezoceramics: Interrelationship between intrinsic and extrinsic factors, J. Eur. Ceram. Soc. 37 (2017) 3501.

[30] R. D. Levi, Dr. Thesis, The Graduate School, Department of Material Science and Engineering, The Pennsylvania State University, Pennsylvania (2009).

[31] U. Yuji, T. Kosuke, K. Takashi, K. Akihide, M. Hiroki, Theoretical analysis of oxygen vacancy formation in Zr-doped $BaTiO_3$, Jpn. J. Appl. Phys. 51 (2012) 09LE01.

[32] T. Shi, L. Xie, L. Gu, J. Zhu, Why Sn doping significantly enhances the dielectric properties of $Ba(Ti_{1-x}Sn_x)O_3$, Sci. Rep. 5 (2015) 8606.

[33] A. K. Kalyani, A. Senyshyn, R. Ranjan, Polymorphic phase boundaries and enhanced piezoelectric response in extended composition range in the lead free ferroelectric $BaTi_{1-x}Zr_xO_3$, J. Appl. Phys. 114 (2013) 014102.

[34] A. K. Kalyani, K. Brajesh, A. Senyshyn, R. Ranjan, Orthorhombic-tetragonal phase coexistence and enhanced piezo-response at room temperature in Zr, Sn, and Hf modified $BaTiO_3$, Appl. Phys. Lett. 104 (2014) 252906.

[35] A. K. Kalyani, H. Krishnan, A. Sen, A. Senyshyn, R. Ranjan, Metastable monoclinic and orthorhombic phases and electric field induced irreversible phase transformation at room temperature in the lead-free classical ferroelectric $BaTiO_3$, Phys. Rev. B 91 (2015) 104104.

[36] W. Liu, X. Ren, Large piezoelectric effect in Pb-free ceramics, Phys. Rev. Lett. 103 (2009) 257602.

[37] L. Dong, D. S. Stone, R. S. Lakes, Enhanced dielectric and piezoelectric properties of $xBaZrO_3$-$(1-x)BaTiO_3$ ceramics, J. Appl. Phys. 111 (2012) 084107.

[38] H. Rietveld, A profile refinement method for nuclear and magnetic structures, J. Appl. Crystallogr. 2 (1969) 65-71.

[39] J. Rodríguez-Carvajal, Recent advances in magnetic structure determination by neutron powder diffraction, Physica B 192 (1993) 55-69.

[40] G. Viola, T. Saunders, X. Wei, K. B. Chong, H. Luo, M. J. Reece, H. Yan, Contribution of piezoelectric effect, electrostriction and ferroelectric/ferroelastic switching to strain-electric field response of dielectrics, J. Adv. Dielectr. 3 (2013) 1350007.

[41] G. Arlt, P. Sasko, Domain configuration and equilibrium size of domains in BaTiO$_3$ ceramics, J. Appl. Phys. 51 (1980) 4956-4960.

[42] G. Arlt, Twinning in ferroelectric and ferroelastic ceramics: stress relief, J. Mater. Sci. 25 (1990) 2655-2666.

[43] V. V. Shvartsman, A. L. Kholkin, Domain structure of 0.8Pb(Mg$_{1/3}$Nb$_{2/3}$)O$_3$-0.2PbTiO$_3$ studied by piezoresponse force microscopy, Phys. Rev. B 69 (2004) 014102.

[44] S. Lin, T. Lü, C. Jin, X. Wang, Size effect on the dielectric properties of BaTiO$_3$ nanoceramics in a modified Ginsburg-Landau-Devonshire thermodynamic theory, Phys. Rew. B 74 (2006) 134115.

[45] B. Zalar, V. V. Laguta, R. Blinc, NMR evidence for the coexistence of order-disorder and displacive components in barium titanate, Phys. Rev. Lett. 90 (2003) 037601.

[46] U. M. Pasha, H. Zheng, O. P. Thakur, A. Feteira, K. R. Whittle, D. C. Sinclair, I. M. Reaney, *In situ* Raman spectroscopy of A-site doped barium titanate, Appl. Phys. Lett. 91 (2007) 062908.

[47] J. P. Sokoloff, L. L. Chase, D. Rytz, Direct observation of relaxation modes in KNbO$_3$ and BaTiO$_3$ using inelastic light scattering, Phys. Rev. B 38 (1988) 597-605.

[48] U. D. Venkateswaran, V. M. Naik, R. Naik, High-pressure Raman studies of polycrystalline BaTiO$_3$, Phys. Rev. B 58 (1998) 14256-14260.

[49] R. Z. Tai, K. Namikawa, A. Sawada, M. Kishimoto, M. Tanaka, P. Lu, K. Nagashima, H. Maruyama, M. Ando, Picosecond view of microscopic-scale polarization clusters in paraelectric BaTiO$_3$, Phys. Rev. Lett. 93 (2004) 087601.

[50] X. Wei, Y. Feng, X. Yao, Dielectric relaxation behavior in barium stannate titanate ferroelectric ceramics with diffused phase transition, Appl. Phys. Lett. 83 (2003) 2031-2033.

[51] M. Deluca, L. Stoleriu, L. P. Curecheriu, N. Horchidan, A. C. Ianculescu, C. Galassi, L. Mitoseriu, High-field dielectric properties and Raman spectroscopic investigation of the ferroelectric-to-relaxor crossover in BaSn$_x$Ti$_{1-x}$O$_3$ ceramics, J. Appl. Phys. 111 (2012) 084102.

[52] M. T. Buscaglia, M. Viviani, V. Buscaglia, L. Mitoseriu, A. Testino, P. Nanni, Z. Zhao, M. Nygren,

C. Harnagea, D. Piazza, C. Galassi, High dielectric constant and frozen macroscopic polarization in dense nanocrystalline BaTiO$_3$ ceramics, Phys. Rev. B 73 (2006) 064114.

[53] V. V. Shvartsman, W. Kleemann, J. Dec, Z. K. Xu, S. G. Lu, Diffuse phase transition in BaTi$_{1-x}$Sn$_x$O$_3$ ceramics: An intermediate state between ferroelectric and relaxor behavior, J. Appl. Phys. 99 (2006) 124111.

[54] B. S. Kang, S. K. Choi, C. H. Park, Diffuse dielectric anomaly in perovskite-type ferroelectric oxides in the temperature range of 400–700 °C, J. Appl. Phys. 94 (2003) 1904-1911.

[55] R. Scharfschwerdt, A. Mazur, O. F. Schirmer, H. Hesse, S. Mendricks, Oxygen vacancies in BaTiO$_3$, Phys. Rev. B 54 (1996) 15284-15290.

[56] Z. Shen, H. Yan, D. Gruner, L. M. Belova, Y. Sakamoto, J. Hu, C. W. Nan, T. Hoche, M. J. Reece, Ferroelectric ceramics with enhanced remnant polarization by ordered coalescence of nano-crystals, J. Mater. Chem. 22 (2012) 23547-23552.

[57] H. Yan, F. Inam, G. Viola, H. Ning, H. Zhang, Q. Jiang, T. Zeng, Z. Gao, M. J. Reece, The contribution of electrical conductivity, dielectric permittivity and domain switching in ferroelectric hysteresis loops, J. Adv. Dielectr. 1 (2011) 107-118.

[58] D. Wang, A. A. Bokov, Z. G. Ye, J. Hlinka, L. Bellaiche, Subterahertz dielectric relaxation in lead-free Ba(Zr,Ti)O$_3$ relaxor ferroelectrics, Nat. Comm. 7 (2016) 11014.

[59] V. Koval, G. Viola, Y. Tan, in *Ferroelectric Materials - Synthesis and Characterization* (ed Aime Pelaiz Barranco) Ch. 09 InTech (2015).

[60] L. He, D. Vanderbilt, First-principles study of oxygen-vacancy pinning of domain walls in PbTiO$_3$, Phys. Rev. B 68 (2003) 134103.

[61] J. F. Scott, M. Dawber, Oxygen-vacancy ordering as a fatigue mechanism in perovskite ferroelectrics, Appl. Phys. Lett. 76 (2000) 3801-3803.

[62] F. Li, S. Zhang, Z. Xu, L. Q. Chen, The Contributions of polar nanoregions to the dielectric and piezoelectric responses in domain-engineered relaxor-PbTiO$_3$ crystals, Adv. Funct. Mater. 27

(2017) 1700310.

[63] J. Petzelt, Dielectric grain-size effect in high-permittivity ceramics, Ferroelectrics 400 (2010) 117-134.

[64] Wook Jo, Robert Dittmer, Matias Acosta, Jiadong Zang, Claudia Groh, Eva Sapper, Ke Wang, Jürgen Rödel, Giant electric-field-induced strains in lead-free ceramics for actuator applications - status and perspective, J. Electroceram. 29 (2012) 71-93.

[65] Y. Tan, J. Zhang, C. Wang, G. Viola, H. Yan, Enhancement of electric field-induced strain in BaTiO$_3$ ceramics through grain size optimization, Phys. Status Solidi A 212 (2015) 433-438.

[66] A. A. Bokov, Z. G. Ye, Recent progress in relaxor ferroelectrics with perovskite structure, J. Mater. Sci. 41(2006) 31-52.

[67] L. E. Cross, Relaxor ferroelectrics, Ferroelectrics 76 (1987) 241-267.

[68] D. Bolten, U. Böttger, R. Waser, Reversible and irreversible piezoelectric and ferroelectric response in ferroelectric ceramics and thin films, J. Eur. Ceram. Soc. 24 (2004) 725-732.

[69] D. Damjanovic, Contributions to the piezoelectric effect in ferroelectric single crystals and ceramics, J. Am. Ceram. Soc. 88 (2005) 2663-2676.

[70] J. Glaum, T. Granzow, J. Rödel, Evaluation of domain wall motion in bipolar fatigued lead-zirconate-titanate: A study on reversible and irreversible contributions, J. Appl. Phys. 107 (2010) 104119.

[71] X. Ren, Large electric-field-induced strain in ferroelectric crystals by point-defect-mediated reversible domain switching, Nat. Mater. 3 (2004) 91-94.

[72] E. Burcsu, G. Ravichandran, K. Bhattacharya, Large strain electrostrictive actuation in barium titanate, Appl. Phys. Lett. 77 (2000) 1698-1700.

[73] W. Cao, Ferroelectrics: The strain limits on switching, Nat. Mater. 4 (2005) 727-728.

**Figure 1**. SEM images of BTS ceramics sintered at 1160 ℃ (a); 1200 ℃ (b); 1240 ℃ (c); 1280 ℃ (d) and 1320 ℃ (e). The average grain size, as calculated for the ceramics, is plotted as a function of the sintering temperature in (f).

**Figure 2**. (a) Dark-field TEM image of BTS ceramics sintered at 1160 °C (a). A, B, C and D denote the positions at which the SAED patterns shown in (A), (B), (C) and (D), respectively, were obtained. (b) Bright-field transmission electron microscopy image of Sn-doped $BaTiO_3$ obtained from the area marked by the black dotted line in (a). E and F denote positions at which the SAED patterns shown in (E) and (F), respectively, were obtained. All SAED patterns were indexed in the tetragonal unit cell (white indices), patterns (B) and (C) were additionally indexed in a rhombohedral unit cell (blue indices). Extra spots on SAED pattern (E) are marked with white arrows.

**Figure 3**. Topography of polished surface of BTS1160 ceramic (a); PFM phase images of BTS1160 ceramic (b); selected area for the PFM line scanning (c) and corresponding line profile analyses for the BTS1160 ceramic (d); Topography of polished surface of the BTS1280 sample (e); PFM phase images of BTS1280 (f); selected area for the PFM line scanning (g) and corresponding line profile analyses for the BTS1280 ceramic (h).

**Figure 4**. Phase composition of the BTS ceramics at -100 °C (a), 25 °C (b) and 75 °C (c), as obtained from the Rietveld refinement of the XRD data.

**Figure 5**. Temperature dependence of the relative dielectric permittivity and loss of BTS ceramics sintered at three different temperatures (a, b – 1160 °C; c, d – 1280 °C and e, f – 1320 °C) and measured at 1 kHz, 10 kHz, 100 kHz and 1 MHz (a-f). Temperature dependence of the relative dielectric permittivity and loss of BTS ceramics with different grain size measured at 1kHz (g,h).

**Figure 6**. Polarization-electric field and current-electric field curves for BTS1160, BTS1240 and BTS1320 measured at 25 °C (a - c) and 125 °C (d - f); temperature dependences of $P_{max}$ and $P_r$ for BTS ceramics sintered at different temperatures (g).

**Figure 7**. Bipolar (a) and unipolar (b) electric field-induced strain behaviour of BTS ceramics with different grain sizes; (c) strain vs. polarization curves for BTS ceramics with different grain sizes.

**Figure 8**. Grain size dependence of the permittivity of as-prepared (unpoled) BTS ceramics at different temperatures (a); grain size dependence of the permittivity of as-prepared (unpoled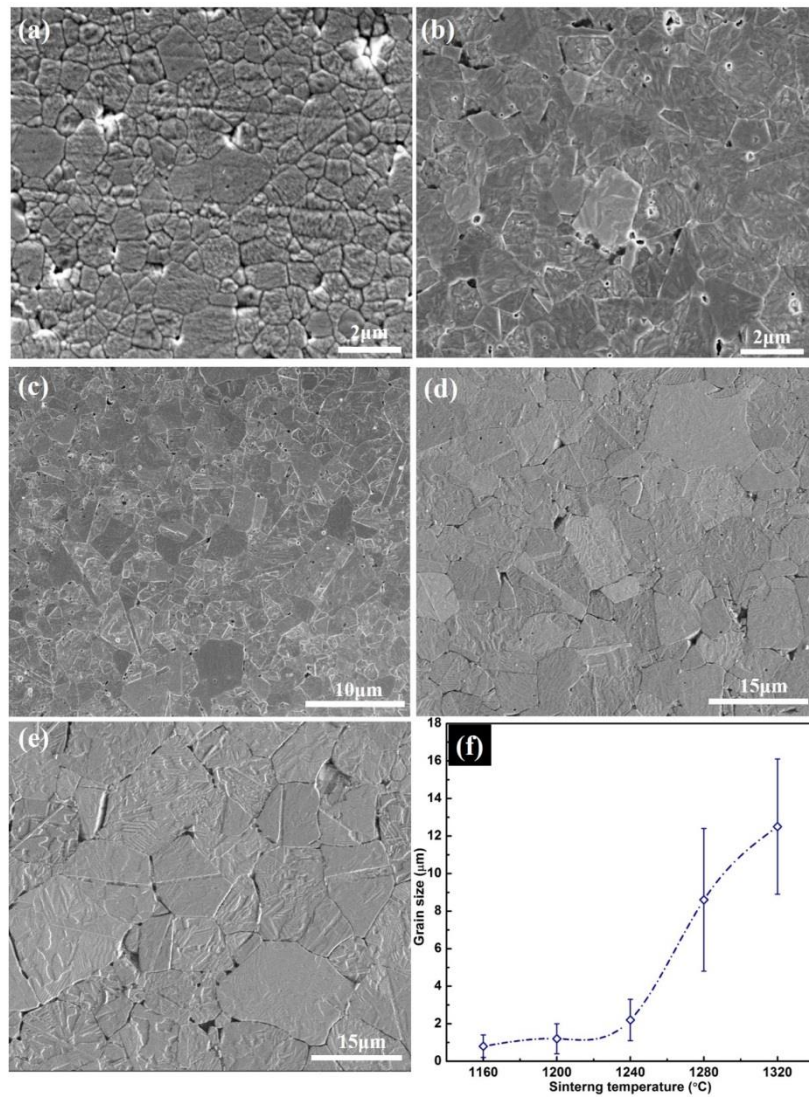) and poled BTS ceramics at room temperature (b); grain size dependence of $d_{33}$ of BTS ceramics at different temperatures (c); grain size dependence of $d_{33}^{*}$ of as-prepared (unpoled) and poled BTS ceramics at room temperature (d).

**Figure 1**

**Figure 2**
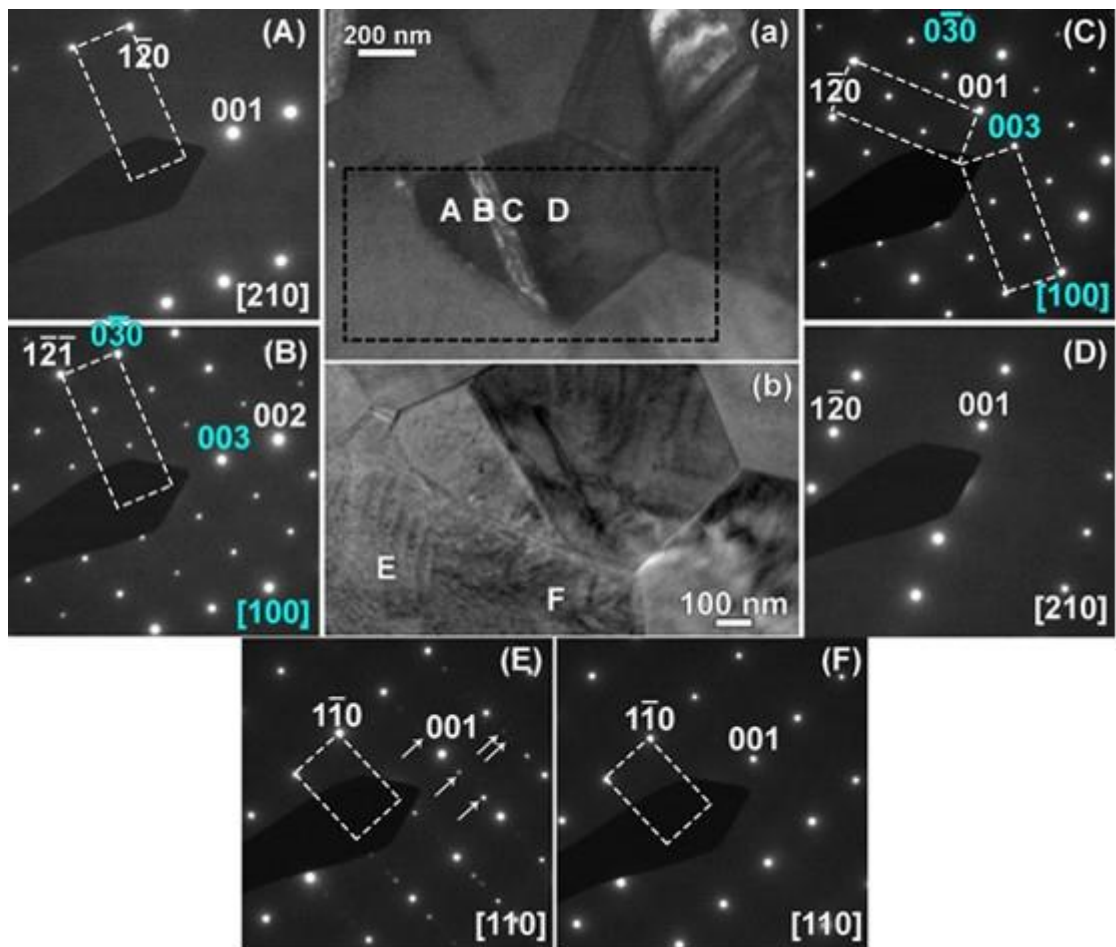
**Figure 3**
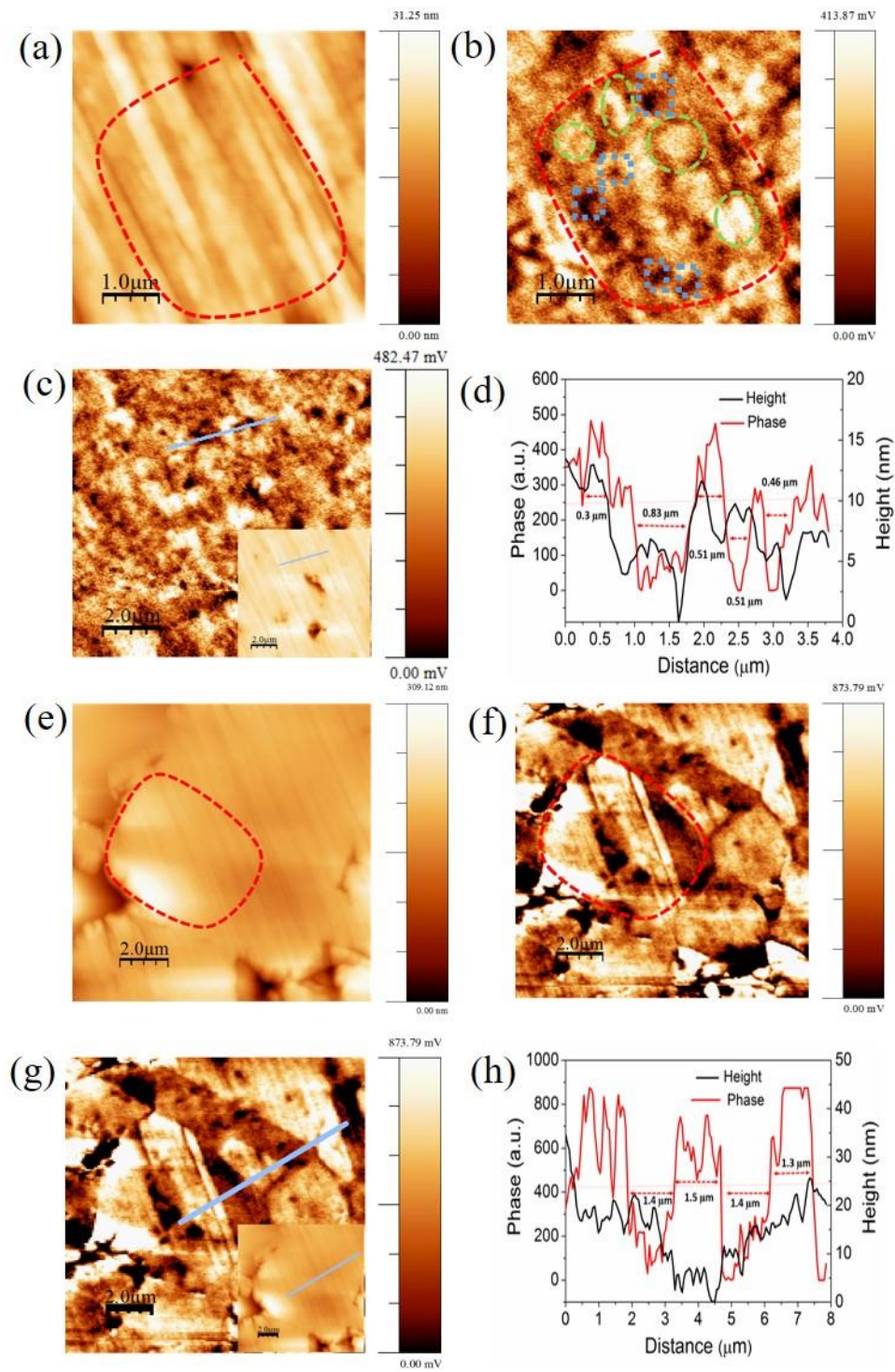
**Figure 4**
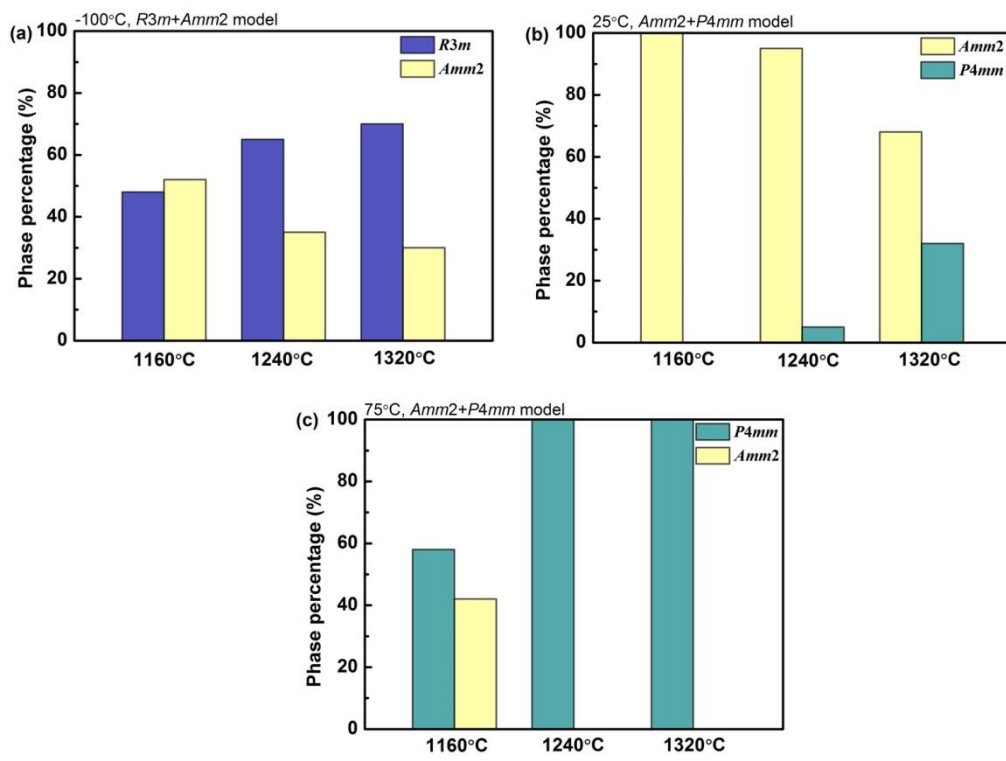
**Figure 5**
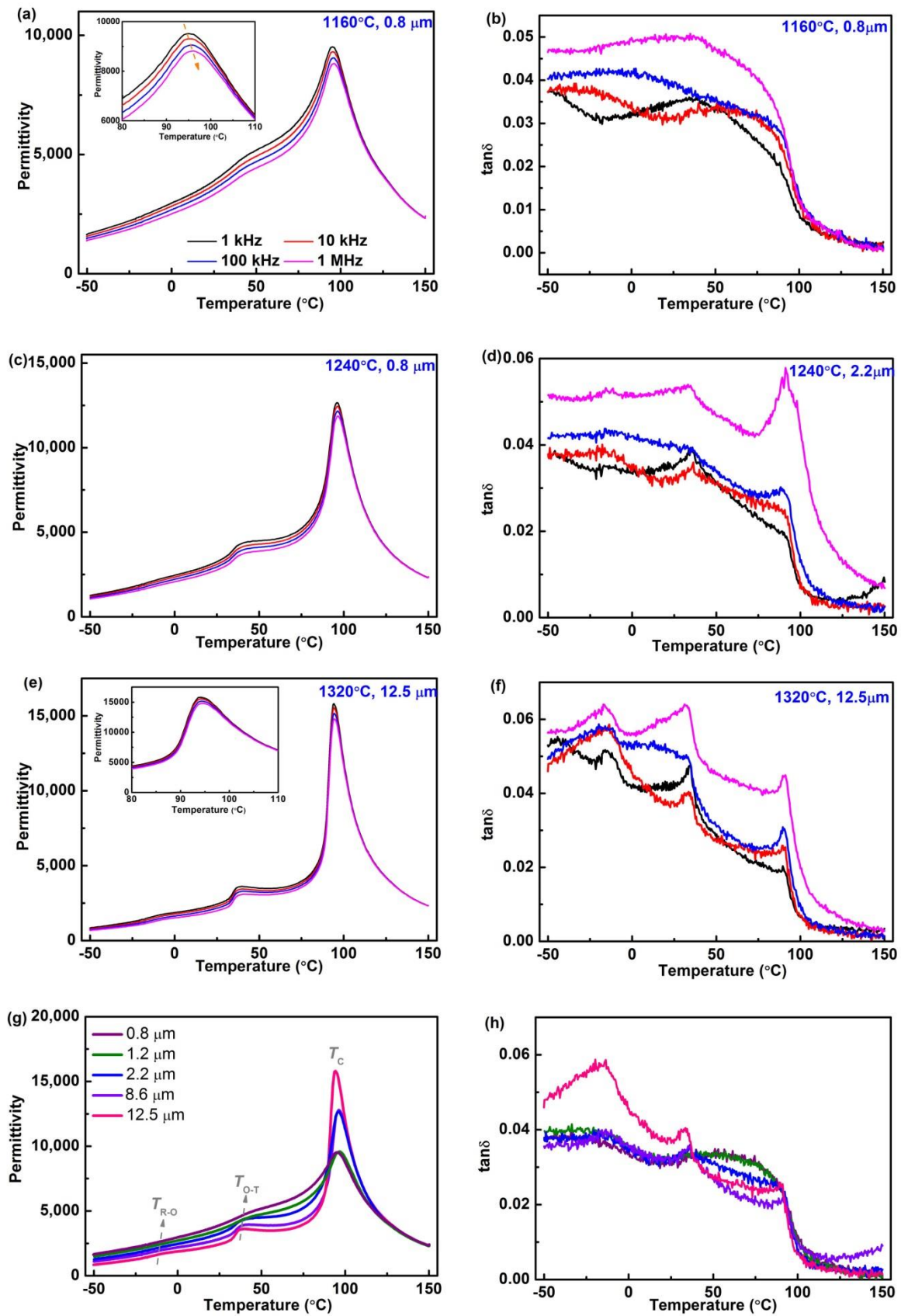
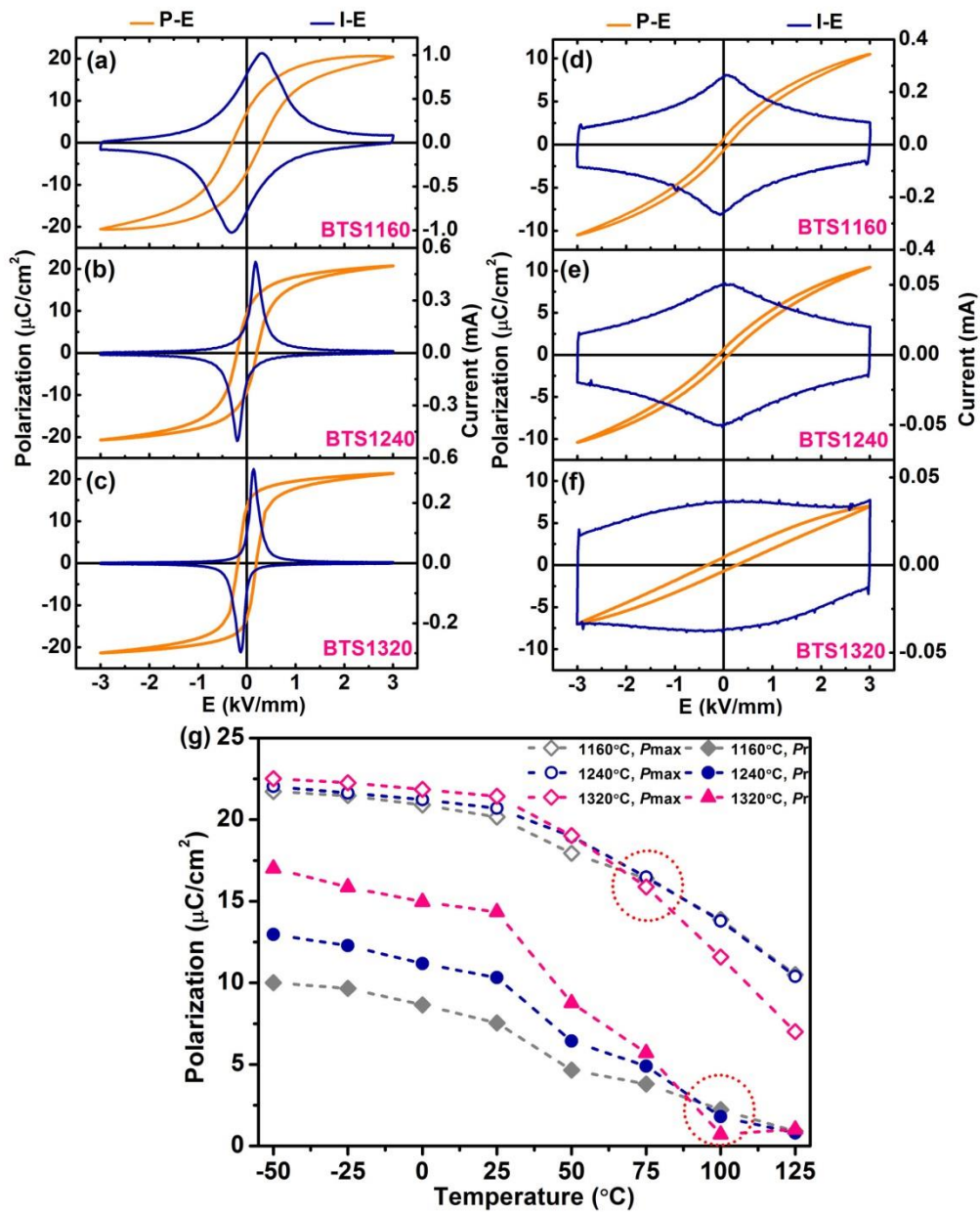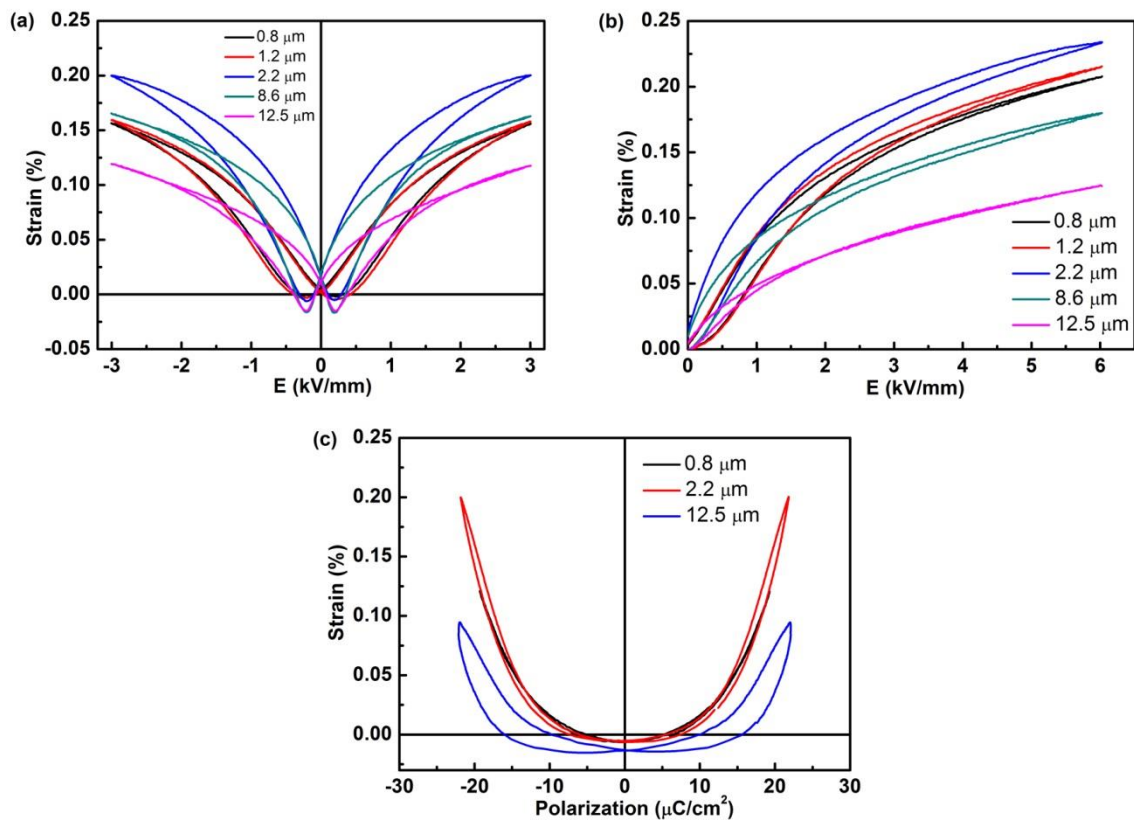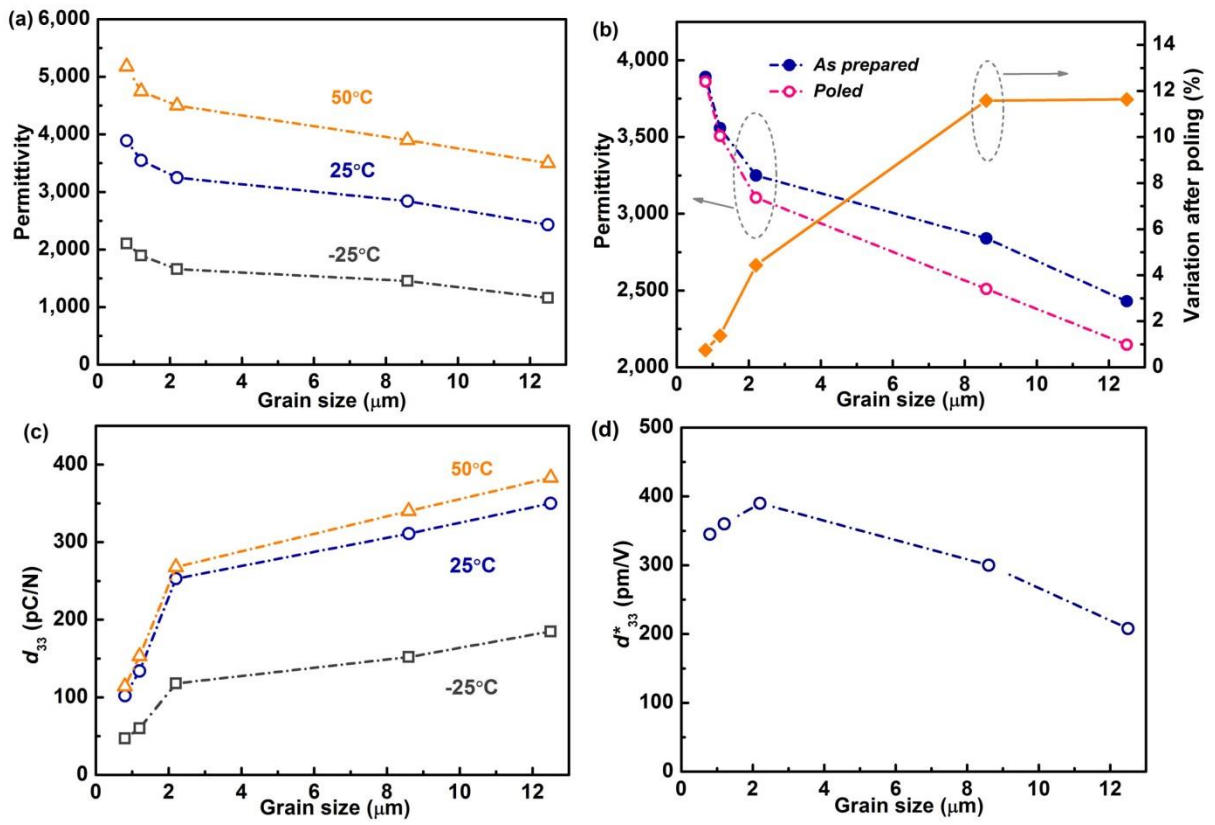**Figure 6**

**Figure 7**

**Figure 8**

**Supplementary material**

# On the origin of grain size effects in Ba(Ti$_{0.96}$Sn$_{0.04}$)O$_3$ perovskite ceramics

Yongqiang Tan, [1,2] Giuseppe Viola, [3,4] Vladimir Koval,[5] Chuying Yu,[3] Amit Mahajan,[3] Jialiang Zhang,[2] Haibin Zhang,[1, *] Xiaosong Zhou,[1] Nadezda V. Tarakina,[3] and Haixue Yan[3,*]

[1]*Innovation Research Team for Advanced Ceramics, Institute of Nuclear Physics and Chemistry, China Academy of Engineering Physics, Mianyang, 621900, China*
[2]*School of Physics, State Key Laboratory of Crystal Materials, Shandong University, Jinan, 250100, China*
[3]*School of Engineering and Materials Science, Queen Mary University of London, Mile End Road, London, E1 4NS, United Kingdom*
[4]*Department of Applied Science and Technology, Institute of Materials Physics and Engineering, Corso Duca Degli Abruzzi 24, 10129 Torino, Italy*
[5]*Institute of Materials Research, Slovak Academy of Sciences, Watsonova, 47, 040 01 Kosice, Slovakia*

**Table S1.** Refined lattice parameters of individual structural phases and reliability *R*-factors obtained from the Rietveld analysis of the XRD data, as collected at -100 ℃, 25 ℃, 75 ℃ and 147 ℃.

| Test temperature | Phase | Lattice parameters (Ang) | | | R-factors ($R_p$, $R_{wp}$) | | |
|---|---|---|---|---|---|---|---|
| | | BTS1160 | BTS1240 | BTS1320 | BTS 1160 | BTS 1240 | BTS 1320 |
| **-100 °C** | *R3m* | a=5.6702(4) c=6.9441(1) | a=5.6669(0) c=6.9579(1) | a=5.6603(6) c=6.9582(1) | 6.5, 8.9 | 6.5, 8.9 | 10.2, 13.0 |
| | *Amm2* | a=3.9957(2) b=5.6903(5) c=5.6808(5) | a=3.9932(2) b=5.6853(6) c=5.6977(6) | a=3.9955(3) b=5.6914(7) c=5.6799(7) | | | |
| **25 °C** | *Amm2* | a=3.9968(6) b=5.705(2) c=5.688(2) | a=4.00327(6) b=5.6808(2) c=5.6851(2) | a=3.9988(1) b=5.6892(4) c=5.6978(4) | 8.6, 11.1 | 9.7, 12.6 | 10.1, 13.4 |
| | *P4mm* | | a=4.00916(5) c=4.02510(7) c/a ≈ 1.0040 | a=4.00839(7) c=4.0253(1) c/a ≈ 1.0042 | | | |
| **75 °C** | *P4mm* | a=4.01125(1) c=4.0239(3) c/a ≈ 1.0028 | a=4.01037(3) c=4.02577(4) c/a ≈ 1.0038 | a=4.00966(2) c=4.02630(3) c/a ≈ 1.0042 | 7.9, 10.8 | 8.2,10.9 | 8.9, 11.5 |
| | *Amm2* | a=4.0009(3) b=5.7012(1) c=5.6964(1) | | | | | |
| **147 °C** | *Pm-3m* | a=4.0186(2) | a=4.0180(2) | a=4.0178(2) | 7.4, 10.4 | 7.6, 10.4 | 8.6, 11.3 |
| | *P4mm* | a=4.0198(1) c=4.0216(2) | a=4.018(1) c=4.0200(3) | a=4.018(1) c=4.0193(1) | | | |

| | BTS1160 | BTS1240 | BTS1320 |
|---|---|---|---|
| **Model: *Pm*-3*m*+*P4mm*+*Fm*-3*m*** | | | |
| *Phase*: *Pm*-3*m* | | | |
|    **Fraction (wt. %)** | 94.8(2) | 94.6(2) | 97.4(1) |
|    **Lattice parameters (Å)** | *a=b=c=*4.0186(2) | *a=b=c=*4.0180(2) | *a=b=c=*4.0178(2) |
| | *c/a*=1 | *c/a*=1 | *c/a*=1 |
| | *V*=64.90(1) Å$^3$ | *V*=64.87(1) Å$^3$ | *V*=64.86(1) Å$^3$ |
|    **Calculated density (g/cm³)** | 5.97 | 5.97 | 5.97 |
|    **Atomic coordinates (*X,Y,Z*)** | Ba [0.5,0.5,0.5] | Ba [0.5,0.5,0.5] | Ba [0.5,0.5,0.5] |
| | Ti [0,0,0] | Ti [0,0,0] | Ti [0,0,0] |
| | O [0.5,0,0] | O [0.5,0,0] | O [0.5,0,0] |
|    **Bond lengths (Å)** | Ba – O  2.8416(0) | Ba – O  2.8411(0) | Ba – O  2.8414(0) |
| | Ba – Ti  3.4802(0) | Ba – Ti  3.4797(0) | Ba – Ti  3.4795(0) |
| | Ti – O  2.0093(0) | Ti – O  2.0089(0) | Ti – O  2.0089(0) |
| *Phase*: *P4mm* | | | |
|    **Fraction (wt. %)** | 2.0(2) | 2.0(2) | 0.2(4) |
|    **Lattice parameters (Å)** | *a=b=*4.0198(1) | *a=b=*4.0180(1) | *a=b=*4.0179(2) |
| | *c*=4.0216(2) | *c*=4.0200(3) | *c*=4.0198(1) |
| | *c/a*≈1.0005 | *c/a*≈1.0005 | *c/a*≈1.0005 |
| | *V*=64.98(1) Å$^3$ | *V*=64.90(1) Å$^3$ | *V*=64.89(1) Å$^3$ |
|    **Calculated density (g/cm³)** | 5,97 | 5.96 | 5.97 |
|    **Atomic coordinates (*X,Y,Z*)** | Ba [0,0,0] | Ba [0,0,0] | Ba [0,0,0] |
| | Ti [0,0,0.5323(18)] | Ti [0,0,0.533(2)] | Ti [0,0,0.5432(18)] |
| | O1 [0.5,0.5,0,084(3)] | O1 [0.5,0.5,-0,050(9)] | O1 [0.5,0.5,-0,053(4)] |
| | O2 [0.5,0,0.666(3)] | O2 [0.5,0,0.547(4)] | O2 [0.5,0,0.675(3)] |
|    **Bond lengths (Å)** | Ba – O1 2.8624(14) | Ba – O1 2.8497(46) | Ba – O1 2.8491(12) |
| | Ba – O2 2.4174(64) | Ba – O2 2.413(71) | Ba – O2 2.3963(66) |
| | Ba – Ti  3.4084(10) | Ba – Ti  3.4057(45) | Ba – Ti  3.2827(39) |
| | Ti – O1  1.803(14) | Ti – O1  1.680(43) | Ti – O1  1.623(21) |
| | Ti – O2  2.0806(36) | Ti – O2  2.0800(35) | Ti – O2  2.0776(36) |
|    **Bond angles (deg.)** | O2–Ti–O2 133.09(5) | O2 – Ti – O2 132.98(8) | O2–Ti–O2 133.13(7) |
| *Phase: Fm*-3*m* (*Pt holder*) | | | |
|    **Fraction (wt. %)** | 3.2(1) | 3.3(1) | 2.4(1) |
|    **Lattice parameters (Å)** | *a=b=c=*3.9361(2) | *a=b=c=*3.9344(2) | *a=b=c=*3.9345(1) |
| | *V* = 60.98(0) Å$^3$ | *V* = 60.90(1) Å$^3$ | *V* = 60.91(1) Å$^3$ |
|    **Calculated density (g/cm³)** | 10.62 | 10.64 | 10.63 |
|    **Atomic coordinates (*X,Y,Z*)** | Pt [0,0,0] | Pt [0,0,0] | Pt [0,0,0] |
| *No. of refined parameters* | 41 | 41 | 41 |
| *R-factors ($R_w$, $R_{wp}$)* | 7.4, 10.4 | 7.6, 10.4 | 8.6, 11.3 |
| *Goodness of fit, GOF ($\chi^2$)* | 1.49 | 1.75 | 1.89 |

**Table S3.** Structural parameters, selected bond lengths and *R*-factors for the BTS1160, BTS1240, and BTS1320 samples, as obtained from the Rietveld analysis of the XRD data collected above the Curie temperature (at 147 °C) considering only the *Pm*-3*m* cubic phase of Sn-BaTiO$_3$ (*Fm*-3*m* corresponds to the cubic phase of the Pt holder used in XRD experiments at elevated temperatures).

| | BTS1160 | BTS1240 | BTS1320 |
|---|---|---|---|
| **Model: *Pm*-3*m*+*Fm*-3*m*** | | | |
| ***Phase*: *Pm*-3*m*** | | | |
| Fraction (wt. %) | >95 | >95 | >95 |
| Lattice parameters (Å) | *a*=*b*=*c*=4.0186(0) | *a*=*b*=*c*=4.0179(1) | *a*=*b*=*c*=4.0178(0) |
| | *V*=64.90(0) Å$^3$ | *V*=64.86(1) Å$^3$ | *V*=64.86(0) Å$^3$ |
| Calculated density (g/cm$^3$) | 5.97 | 5.97 | 5.97 |
| Atomic coordinates (*X,Y,Z*) | Ba [0.5,0.5,0.5] | Ba [0.5,0.5,0.5] | Ba [0.5,0.5,0.5] |
| | Ti [0,0,0] | Ti [0,0,0] | Ti [0,0,0] |
| | O [0.5,0,0] | O [0.5,0,0] | O [0.5,0,0] |
| Bond lengths (Å) | Ba – O  2.8416(0) | Ba – O  2.8411(0) | Ba – O  2.841(0) |
| | Ba – Ti  3.4802(0) | Ba – Ti  3.4796(0) | Ba – Ti  3.4795(0) |
| | Ti – O  2.0093(0) | Ti – O  2.0089(0) | Ti – O  2.0089(0) |
| ***Phase: *Fm*-3*m* (Pt holder)*** | | | |
| Fraction (wt. %) | <5 | <5 | <5 |
| Lattice parameters (Å) | *a*=*b*=*c*=3.9358(2) | *a*=*b*=*c*=3.9347(3) | *a*=*b*=*c*=3.9333(3) |
| | *V* = 60.97(0) Å$^3$ | *V* = 60.92(1) Å$^3$ | *V* = 60.85(1) Å$^3$ |
| Calculated density (g/cm$^3$) | 10.63 | 10.64 | 10.63 |
| Atomic coordinates (*X,Y,Z*) | Pt [0,0,0] | Pt [0,0,0] | Pt [0,0,0] |
| | | | |
| ***No. of refined parameters*** | 27 | 27 | 27 |
| ***R*-factors (*R$_w$*, *R$_{wp}$*)** | 8.14, 11.1 | 15.0, 19.7 | 10.6, 13.8 |
| ***Goodness of fit, GOF ($\chi^2$)*** | 2.14 | 5.62 | 3.16 |
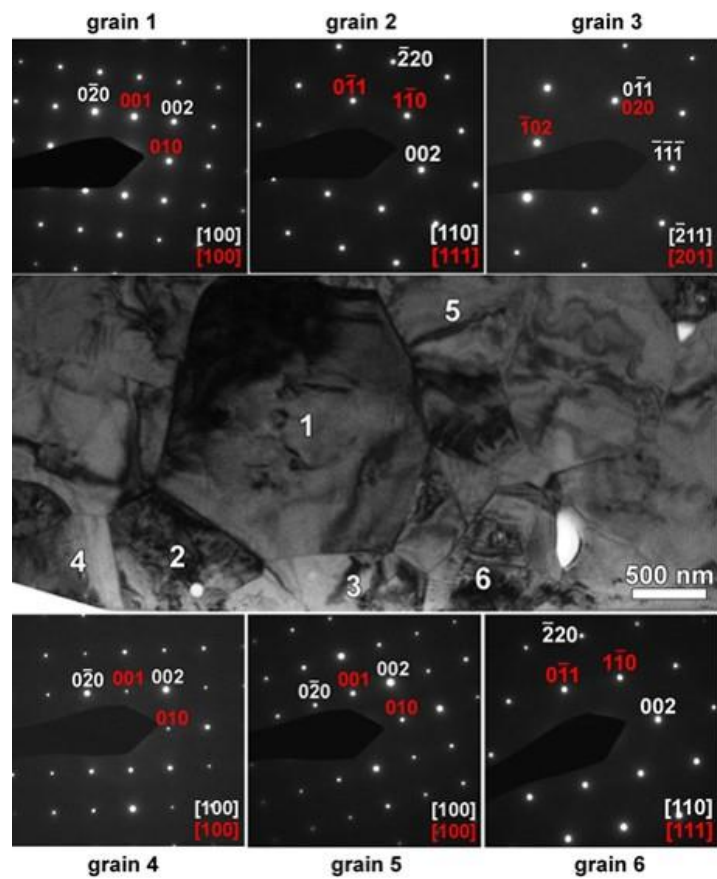
Figure S1. Bright-field transmission electron microscopy image of BTS1160 ceramic and SAED patterns obtained from the grains marked by the numbers. All SAEDs are indexed in the orthorhombic (white indexes) and the cubic (red indexes) unit cells.
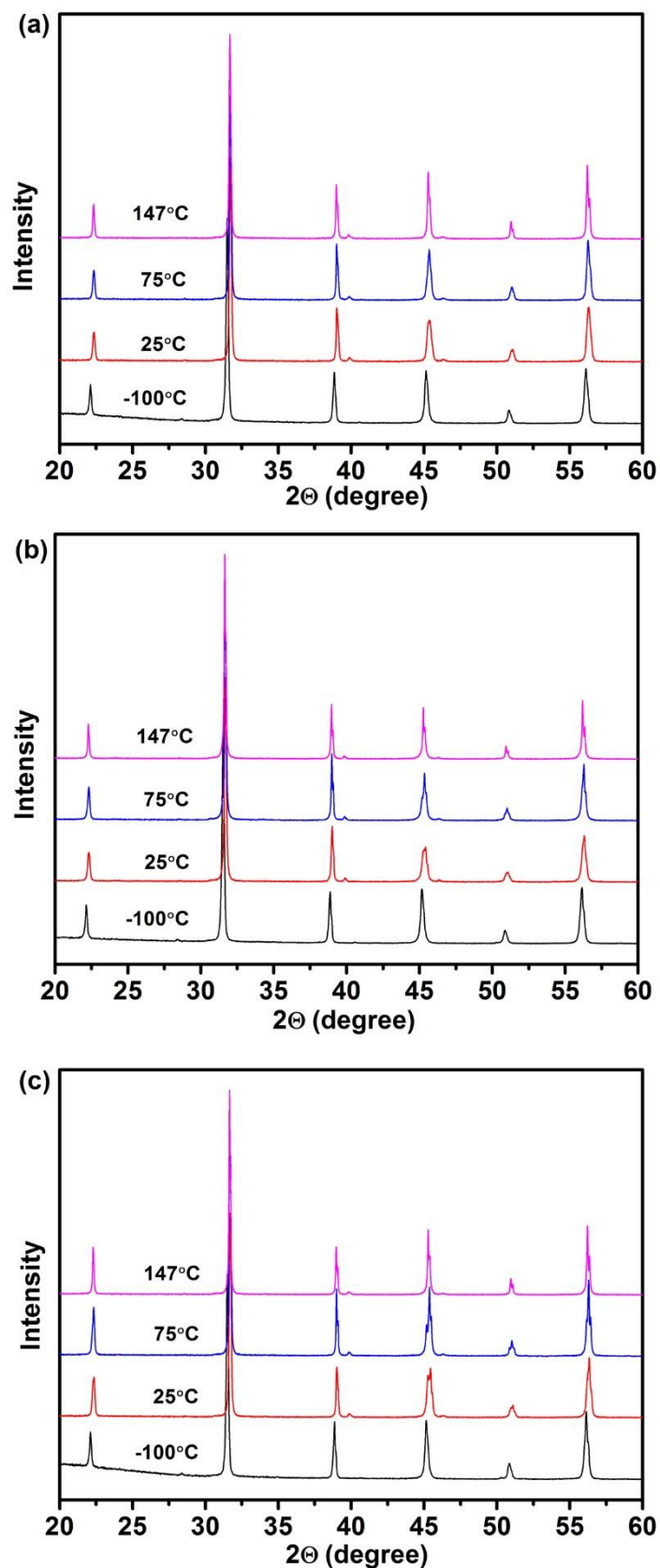
**Figure S2**. Evolution of the XRD patterns with increasing temperature from -100 °C to 147 °C for BTS ceramics sintered at (a) 1160 °C; (b) 1240 °C; (c) 1320 °C. (Note: Small peaks at 39.7° and 46.2° are reflections from the cubic (111) and (200) planes of the Pt holder.)

Fig. S3 shows the representative results of the Rietveld refinements for the BTS1160 sample at 147 $^0$C. Comparing the fitting profiles for the mixed (*Pm-3m+P4mm+Fm-3m*) model and the *Pm-3m+Fm-3m* structural model in the figure and taking into an account the calculated values of the GOF parameter for all the samples (see the last row in Table S2 and Table S3; e.g., $\chi^2$ = 1.49 *vs.* $\chi^2$ = 2.14 for the mixed-phase model and the single-phase model, respectively, for the BTS1160 sample), one can claim that, above the Curie temperature, the Sn-doped BaTiO$_3$ ceramics comprise of the paraelectric *Pm-3m* phase, which is a dominant phase, and a minor tetragonal/pseudo-cubic phase of the *P4mm*-like local objects, represented by polar nanoregions (PNRs).
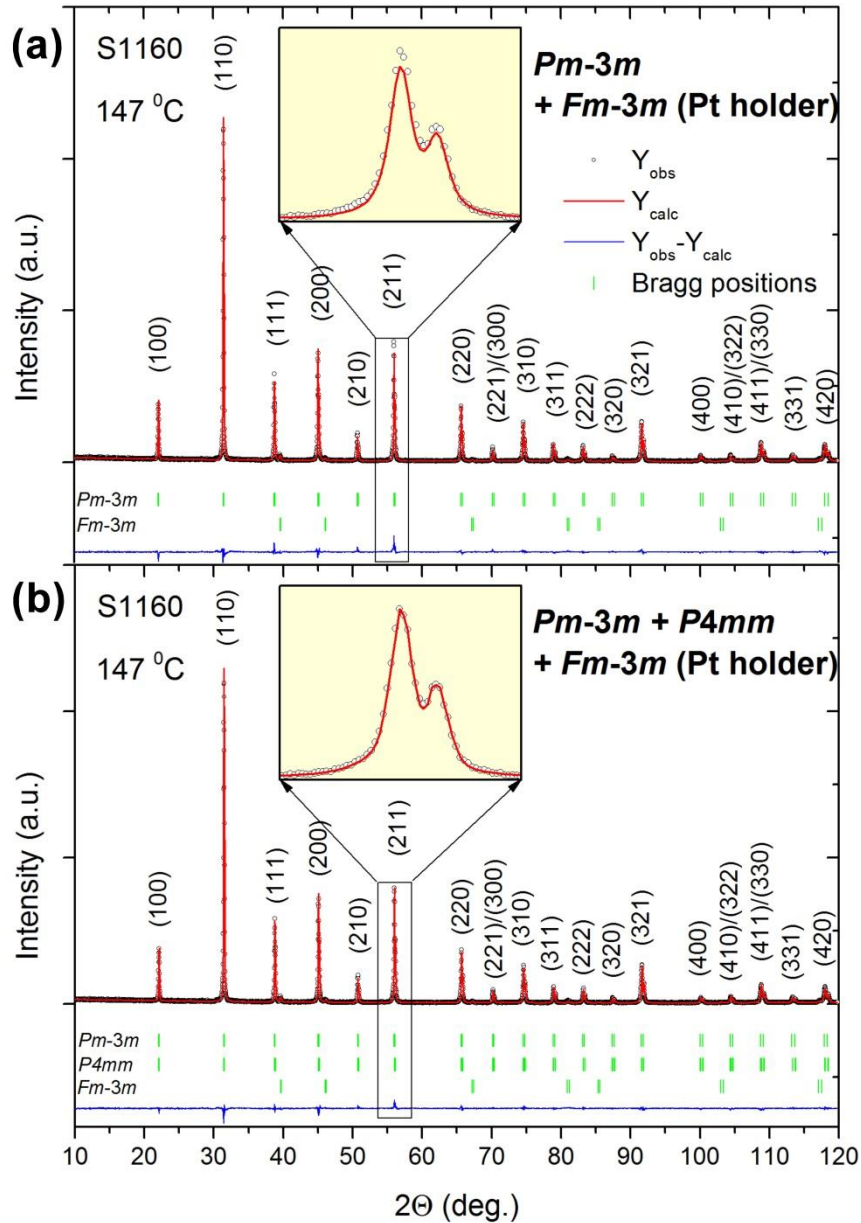


**Figure S3.** Rietveld plot for the refinement of the BTS1160 ceramics in space group a) *Pm-3m*, and b) *Pm-3m+P4mm*. The *Fm-3m* phase represents the Pt holder used in high-temperature measurements. The inset illustrates the enlarged view of the XRD pattern around the (211) peak, indicating the existence of polar nanoregions in the sample above the Curie temperature.
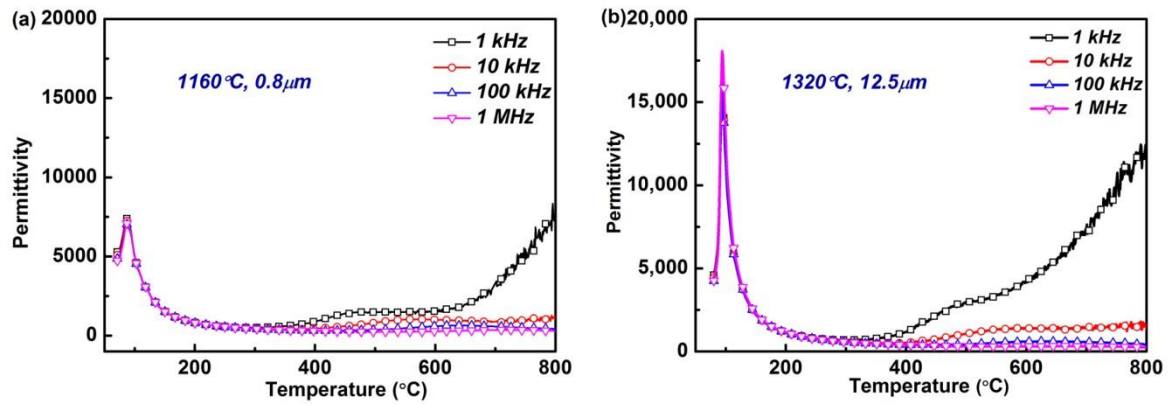
Figure S4. Extended temperature dependence of the relative dielectric permittivity up to 800 °C for BTS ceramics sintered at 1160 °C (a) and 1320 °C (b). The permittivity peaks between 400 °C to 600 °C can be attributed to point defects. The intensity of the peaks is lower than pure $BaTiO_3$ ceramics [1,2].

**References**

[1] B. S. Kang, S. K. Choi, C. H. Park, Diffuse dielectric anomaly in perovskite-type ferroelectric oxides in the temperature range of 400–700 °C, J. Appl. Phys. **94**, 1904 (2003).
[2] Y. Tan, J. Zhang, Y. Wu, C. Wang, V. Koval, B. Shi, H. Ye, R. McKinnon, G. Viola, H. Yan, Unfolding grain size effects in barium titanate ferroelectric ceramics, Sci. Rep. **5**, 9953 (2015).